Atmos. Meas. Tech. Discuss., 8, 3087–3120, 2015
www.atmos-meas-tech-discuss.net/8/3087/2015/
doi:10.5194/amtd-8-3087-2015


Atmospheric Measurement Techniques Discussions
Open Access



# On the potential of 2-D-Video Disdrometer technique to measure micro physical parameters of solid precipitation

**F. Bernauer, K. Hürkamp, W. Rühm, and J. Tschiersch**

Institute of Radiation Protection, Helmholtz Zentrum München, 85764 Neuherberg, Germany

Received: 2 March 2015 – Accepted: 7 March 2015 – Published: 20 March 2015

Correspondence to: F. Bernauer (felix.bernauer@helmholtz-muenchen.de)

Published by Copernicus Publications on behalf of the European Geosciences Union.

## Abstract

Detailed characterization and classification of precipitation is an important task in atmospheric research. Line scanning 2-D-video disdrometer technique is well established for rain observations. The two orthogonal views taken of each hydrometeor passing the sensitive area of the instrument qualify this technique especially for detailed characterization of non symmetric solid hydrometeors. However, in case of solid precipitation problems related to the matching algorithm have to be considered and the user must be aware of the limited spacial resolution when size and shape descriptors are analyzed. This work has the aim of clarifying the potential of 2-D-video disdrometer technique in deriving size, velocity and shape parameters from single recorded pictures. The need of implementing a matching algorithm suitable for mixed and solid phase precipitation is highlighted as an essential step in data evaluation. For this purpose simple reproducible experiments with solid steel spheres and irregularly shaped styrofoam particles are conducted. Self-consistency of shape parameter measurements is tested in 40 cases of real snow fall. As result it was found, that reliable size and shape characterization with a relative standard deviation of less than 5 % is only possible for particles larger than 1 mm. For particles between 0.5 and 1.0 mm the relative standard deviation can grow up to 22 % for the volume, 17 % for size parameters and 14 % for shape descriptors. Testing the adapted matching algorithm with a reproducible experiment with styrofoam particles a mismatch probability of less than 2.5 % was found. For shape parameter measurements in case of real solid phase precipitation the 2DVD shows self-consistent behavior.


## 1 Introduction

Observation of precipitation micro structure is of high interest in many branches of research. The development, improvement and verification of numerical weather prediction models (Xue et al., 2000), radar back scatter computations for microwave fre-





AMTD
8, 3087–3120, 2015

quencies (Hiroshi, 2008) as well as the parametrization of wash out efficiency of particle bound radionuclides and atmospheric pollutants in general (Sportisse, 2007; Kyrö et al., 2009; Paramonov et al., 2011) require detailed characterization and classification of precipitation.

Solid precipitation micro structure can be described by analyzing single hydrometeors conserved on *Formvar* slides in the microscope (Schaefer, 1956). Zikmunda (1972) could observe hydrometeor micro structure together with fall speed by using stereo-photography. Frank et al. (1994) measured rain drop size distributions by using a CCD camera in combination with a proper illumination unit and digital image processing. Ground based observations with so called video disdrometers are a more recent development and meanwhile commonly used because of the large amount of data that can be retrieved in a flexible and low cost way compared to for example airborn particle probe imagers (Feind, 2008). This technique is well established for measurements of rain microphysics (Tokay et al., 2001; Schuur et al., 2001; Thurai and Bringi, 2005; Zhang et al., 2008; Thurai et al., 2009, 2014). Brandes et al. (2007) used 2-D video disdrometer technique for a statistical description of hydrometeors in snowstorms. Huang et al. (2010) developed a methodology to derive radar reflectivity – liquid equivalent snow rate relations and Zhang et al. (2011) described winter precipitation micro physics with a 2-D-video disdrometer. Recently 2-D-video disdrometer technique was used by Grazioli et al. (2014) for an automatic snow event classification. The type of 2-D-video disdrometers as described by Kruger and Krajewski (2002) gives supplementary details due to its two orthogonal views of the detected hydrometeors.

Another type of optical disdrometer which has two parallel light planes is the hydrometeor velocity and shape detector (HVSD) used for size and velocity measurements of liquid and solid phase precipitation (Barthazy et al., 2004; Barthazy and Schefold, 2006). The study from Battaglia et al. (2010) about a comparison between a 2-D-video disdrometer and a Particle Size Velocity (PARSIVEL) disdrometer (Löffler-Mang and Joss, 2000) comes to the conclusion that both instruments have shortcomings in measuring size distributions and fall velocity of solid phase precipitation.





AMTD
8, 3087–3120, 2015

This work has the aim of clarifying the potential of 2-D-video disdrometer technique in deriving size, velocity and shape parameters from single recorded pictures. Previously mentioned studies on solid precipitation deal with statistical descriptions of real case events and lack of a real reference which makes verification difficult. It is the objective of this study that measured size, velocity and shape parameters are compared to known or theoretically calculated values. Easily reproducible experiments with solid steel spheres and styrofoam particles are conducted with a 2-D-video disdrometer and the need of implementing a matching algorithm suitable for mixed and solid phase precipitation is highlighted as an essential step in data evaluation. Furthermore the instrument's self-consistency in 40 real case measurements of snow micro structure will be analyzed.

## 2 Instrument and methods

### 2.1 Principle of operation

The instrument used in this study is a Compact 2-D-Video Disdrometer (2DVD, by Joanneum Research, Graz, Austria; Fig. 1). A schematic view of the 2DVD measurement principle is shown in Fig. 2. The main parts of the device are two illumination units and two CCD line scan cameras. By means of a halogen lamp, a mirror and a Fresnel lens each illumination unit produces an approximately homogenous background light which is scanned by one of the cameras. The combination of the two illumination units and the two cameras result in two planes that enclose an angle of 90° and have a vertical distance of approximately 6 mm. The exact plane distance can be found with a standard calibration procedure recommended by the manufacturer. The area of overlap is approximately 10 cm × 10 cm large and is called the sensitive area. A hydrometeor falling through one of the light planes produces a shadow on a certain amount of pixels in each line. Stacking these lines to a complete picture delivers shape information for every single hydrometeor. A detailed description of an earlier version of the 2DVD and an investigation on its potential in measuring rain parameters can be found in Kruger and Krajewski (2002). The smaller housing design of the Compact 2DVD makes it less sensitive to horizontal winds. Its cameras scan a line containing 632 pixels with a frequency of 55.272 kHz which results in a higher spacial resolution.

## 2.2 The matching problem

Every hydrometeor that falls through the 2DVD within the shaded areas (see Fig. 3) is seen by at least one camera. But only hydrometeors that are seen by both cameras (cross shaded area) can be used for subsequent data analysis. The most critical step in processing 2DVD raw data is finding exactly that pair of pictures that belongs to one and the same hydrometeor. This process is called matching.

In contrast to rain where a well known symmetry and size–velocity relation can be assumed, the shapes of solid and mixed phase hydrometeors are more complex. This makes it more difficult to find a pair of 2DVD images that belongs to the same hydrometeor. Without implementing an appropriate matching algorithm the probability of errors in shape and velocity measurement through matching artifacts is very high. To find the right matching partner to a picture recorded in camera A a time window has to be defined in which the matching partner has to appear in camera B. The narrower the time window the higher is the probability to find the right match. Raindrops have a well known relationship between their size and terminal fall velocity (Gunn and Kinzer, 1949; Atlas et al., 1973) and the time window can be set very narrow. In case of solid phase precipitation the fall velocity depends not only on size but also on shape and degree of riming (Locatelli and Hobbs, 1974; Barthazy and Schefold, 2006).

A first attempt of solving the matching problem for snow measurements was done by Hanesch (1999). In this study the approach of Huang et al. (2010) was applied with few modifications. In principle, several ranges of parameters were defined, which the hydrometeors must match to be identified as a single one. Huang et al. (2010) set a fixed velocity range from 0.5 $\mathrm{m\,s^{-1}}$ to 6.0 $\mathrm{m\,s^{-1}}$ for the whole size range. In this work a dynamic upper bound velocity is used for each hydrometeor with the width $w$. It is set to the velocity $v(w)$ which a raindrop with width $w$ would have (Atlas et al., 1973):

$$v(w) = 9.65 - 10.3 \cdot e^{-0.6 \cdot w} \tag{1}$$

This adjustment makes sure that also partially melted and mixed phase hydrometeors can be matched. Figure 4 summarizes the size velocity relationships for different types of hydrometeors in a size range from 0.5 to 8.0 mm as determined by several investigators. It justifies the assumption of Eq. (1) as upper limit.

With the known scan frequency this time window can be translated into an interval of lines in camera B that has to contain the right matching partner (see the shaded region in Fig. 5). In the example from Fig. 5 three possible matching partners are found within the shaded region. Three so called matching factors are now calculated for each pair of pictures:

- $f_1 = 1 - \frac{|SL_A - SL_B|}{\max(SL_A, SL_B)}$
  with $SL_{A/B}$: number of scanned lines in camera A and B
- if $F \leq 1$: $f_2 = F$, else: $f_2 = 2 - F$
  with $F = \frac{\min(W_{max}, H_{max})}{0.8 \cdot \max(W_{max}, H_{max})}$
- $f_3 = W_{min}/W_{max}$

$W_{max}, H_{max}$ and $W_{min}$ denote the maximum and minimum height and width in each picture. The final matching function is a weighted sum of all three matching factors: $f = 0.6f_1 + 0.2f_2 + 0.2f_3$. The matching partner with the highest $f$ is the best match (see Hanesch (1999) and Huang et al. (2010)).

It is worth mentioning that in this study the newly implemented matching algorithm is applied directly to the raw data streams coming from the cameras. The original matching algorithm supplied by the manufacturer (hereafter referred to as *original matching algorithm*) is explicitly not used for the data analysis in this work. Therefore the algorithm used in this study is not called *rematching*. But in the studies from Huang et al.

(2010) and Grazioli et al. (2014) the term *rematching* lets the reader assume that the original algorithm is used in some stage.

### 2.3 Size, velocity and shape parameters

The result of the matching software is a pair of pictures from each hydrometeor falling through the sensitive area. The great advantage of the 2DVD is that a very detailed set of parameters can be derived from two orthogonal views. For each picture a width ($W$), a height ($H$), a perimeter ($P$) and an area ($A$) can be defined as in Fig. 6. A set of shape characterizing parameters can be assigned to each component of a 2DVD image pair. This work deals with three factors which are commonly used in land use analysis (Jiao and Liu, 2012) and recently also in snow classification (Grazioli et al., 2014).

a. **Elongation:** $E = \frac{\max(W,H)}{\min(W,H)}$

   The elongation describes the ratio between width and height. The more elongated a hydrometeor is, the larger is E. Needles have a large elongation. Rain, graupel particles or dendrites have an elongation of approximately one.

b. **Roundness:** $R = \frac{4A}{\pi(\max(W,H))^2}$

   The roundness is a quantity that describes how well the hydrometeor fills out the area that is enclosed in the circumscribing circle. Needles and dendrites have a low roundness. Rain or graupel particles have a roundness of approximately one.

c. **Shape factor:** $S = \frac{4\pi A}{P^2}$

   The shape factor sets the surface area of a particle in relation to its perimeter. An idealy spherical particle has a shape factor of one. The lower the shape factor the more complex is the surface of the particle. Flakes or dendrites have a low shape factor. The shape factor of rain and graupel particles is approximately one.





AMTD
8, 3087–3120, 2015

On the potential of 2-D-Video Disdrometer technique

F. Bernauer et al.

Another, size describing, set of parameters can be derived with the combination of both camera pictures:

d. The **maximum dimension** $D$ [mm] is the maximum value of width and height seen in both cameras.

e. The **volume** $V$ [$mm^3$] of a hydrometeor is calculated the following way: Every line scan cuts the hydrometeor into slices. The volume of each slice is defined by the area of an ellipse with the length of the shadowed line in each camera as semi axis and the height of the line. The sum of these volumes is the volume of the hydrometeor.

f. The **equivalent diameter** $D_{eqd}$ [mm] is the diameter a sphere with the same volume as the hydrometeor would have.

g. The **vertical fall velocity** $v(D)$ [$m\,s^{-1}$] is the exact plane distance at the (x, y) location of the hydrometeor in the sensitive area divided by the time interval from the first hit in camera A to the first hit in camera B.

An ensemble of hydrometeors that fell during a certain time interval is described with mean values of the mentioned microscopic parameters.

## 2.4 Experimental methods

### 2.4.1 Calibration and validation of shape parameters with solid spheres

Possible misalignment of the optical components due to transport, strong winds and the use of a new data analysis software motivate a recalibration of the device in addition to the calibration done by the manufacturer: Steel spheres with diameters from 0.5 to 10 mm were dropped through the measuring area. For each size between 30 and 70 calibration spheres were released from the same height (0.52 m) above the first camera plane and the values for height and width measured in camera A and B were compared





AMTD
8, 3087–3120, 2015

to the known nominal values for the spheres. For the determination of the size of an object the pixel width $p$ has to be known. It is defined as the actual width of a shaded line divided by the number of shaded pixels $n_{\text{pix}}$ and depends on the exact $x$ and $y$ position of the object and on a size dependent correction factor $f_{\text{corr}}$ supplied by the manufacturer. Because of the individual positions in the sensitive area every detected object has its own pixel width:

$$p = p(x, y) \cdot f_{\text{corr}} \tag{2}$$

Dropping solid spheres from a known height through the sensitive area is also suitable for verification of shape and velocity measurements because of the following reasons:

- The real values of elongation ($E$), roundness ($R$) and shape factor ($S$) are easily determined as $E = R = S = 1$.
- The real values of elongation, roundness and shape factor are independent from the orientation of the object to the recording camera which makes the experiment easily reproducible.
- For spherical objects the expected velocity after a certain distance of free fall can be calculated solving the equation of motion

$$m\frac{\mathrm{d}v}{\mathrm{d}t} = mg - \frac{1}{2}\rho C_{\text{D}} A\, v^2 \tag{3}$$

for Reynolds numbers, $Re$, between 100 and 2000. $m$, $v$ and $A$ are the mass, velocity and surface area of the falling object respectively. $g$ is the gravitational acceleration and $\rho$ the air density. The drag coefficient $C_{\text{D}}$ depends on the Reynolds number and varies approximately linearly from 1.0 for $Re = 100$ to 0.35 for $Re = 2000$.





AMTD
8, 3087–3120, 2015

### 2.4.2 Test of the matching algorithm

The originally implemented analysis software for solid phase precipitation supplied by the manufacturer was evaluated in the following way: As an example a real snow fall event was analyzed with the original matching algorithm on the one hand and the established criteria after Hanesch (1999) (see Table 1) on the other hand. These are mainly geometric criteria which snow flakes must fulfill. In addition particles with velocities larger than $6.0\,\mathrm{m\,s^{-1}}$ (which is not reasonable for snow) were sorted out.

For the evaluation of the performance of the new matching algorithm a reproducible experiment with falling objects that behave like solid or mixed phase precipitation particles was performed. Fourteen irregularly shaped styrofoam particles with different maximum dimensions from 2 to 15 mm (Fig. 7) were dropped through the sensitive area one after the other. This was repeated five times and the mean value of the measured fall velocity was calculated for each size. In a second step an ensemble of styrofoam particles where each size was represented by at least one particle was released at the same time from the same height as in the first step. By comparing the measured velocities in the second step to those from the first step miss matches can easily be identified. The styrofoam particles were coated with a stabilizing spray color to avoid breaking of the particles, when they hit the ground. A mean density of $270.0\,\mathrm{kg\,m^{-3}}$ mas measured for the particles.

### 2.4.3 Real snow flakes

A third method for evaluation of 2DVD performance is measuring shape parameters of real precipitation particles. For 38 one minute intervals of solid phase precipitation the mean values of the measured shape parameters were calculated. One way of independent verification is to test the self-consistency of 2DVD measured shape parameters. Intervals with high mean elongation are expected to have low mean roundness and low mean shape factor and vice versa. Intervals with a low mean shape factor should also have a low mean roundness.





AMTD
8, 3087–3120, 2015

## 3 Results

### 3.1 Calibration

The calibration experiment for the height and width measurements with solid spheres shows that mean height and width are overestimated constantly (Fig. 8, left panel). As summarized in Table 2 the overestimation ranges from 0.35 to 0.38 mm. $m$ and $t$ denote the slope and intercept of the regression line, respectively. $r$ is the correlation coefficient.

The right panel in Fig. 8 shows the results of the size measurements after implementing the following equation as a correction of the pixel width:

$$p = p(x,y) \cdot f_{\text{corr}} - t/n_{\text{pix}} \tag{4}$$

There is good agreement between measured and nominal height for camera A.

### 3.2 Measurement ranges and uncertainties

For the experiments with solid spheres the relative standard deviation for each parameter (Sect. 2.3 a to g) can be calculated (Fig. 9). It varies for the elongation, roundness and shape factor in camera A from 14 % for spheres with a diameter of 0.5 mm to 1.7 % for spheres with a diameter of 10 mm. In camera B it varies from from 6 to 2 %. The height and width can be measured with a relative standard deviation between 18 % for small particles and 1.8 % for larger ones in both cameras. The relative standard deviation for equivalent diameter and volume vary from 7 to 1.5 % and from 22 to 5 %, respectively. For the vertical velocity it stays below 1.5 % in the observed size range.

An important parameter for the whole data analysis procedure is the spacial resolution or the width of a single pixel. Depending on the $x$ and $y$ coordinate of the hydrometeor in the measuring plane (see Fig. 3) for the instrument used in this study the single pixel width varies from 0.15 to 0.25 mm pixel$^{-1}$.





AMTD
8, 3087–3120, 2015

### 3.3 Validation of 2DVD measurements

The measurement results with the solid spheres reveal how well shape, size and velocity information gained with 2DVD measurements reproduce the reality.

a. The 2DVD measures **elongations** very close to $E = 1$ (Fig. 10a and b). At 0.5, 2, 3, 4 and 5 mm outliers can be identified.

b. The measured **roundness** values are very close to $R = 1$. The spread of the single measurements gets higher for smaller spheres (Fig. 10c and d).

c. Figure 10e and f show the **shape factors** measured for the calibration spheres. They are between 0.6 and 0.7. Using a blurring edge filter that spreads over 20 pixels before detecting the perimeter of the object values between 0.90 and 0.95 are measured (Fig. 10 g and h).

d. The slope $m$ and intercept $t$ for the linear regression line between nominal and measured **maximum dimension** are $m = 1.04$ and $t = -0.01$ (Fig. 8).

e. **Equivalent diameters** Fig. 11a and

f. **volumes** are reproduced very well in 2DVD measurements (Fig. 11b).

g. Measurements of the **fall velocity** show a very low spread around the theoretically predicted values (Fig. 11c).

Testing the new matching algorithm with an ensemble of styrofoam particles shows the following result. The velocities measured in the ensemble, where all the particles were released at the same time from the same height, have a very low spread around the single measurements, when the particles were released one after the other (Fig. 12). The measured velocities are between 2.0 and 2.9 $\mathrm{m\,s^{-1}}$. Out of 41 detected particles only for the size between 8 and 9 mm one outlier has been detected.

Analyzing the original matching result for a real snow fall event on the contribution of hydrometeors with unreasonable geometry and velocity yields that the original data





AMTD
8, 3087–3120, 2015

set contains 41 % of particles with a maximum dimension above the mean spacial resolution of 0.2 mm, 20 % of particles that additionally pass the geometry filter, 32 % of particles with velocities between 0.5 and 6.0 $\mathrm{m\,s^{-1}}$ and only 25 % of particles with velocities lower than the velocity a raindrop with the same maximum dimension would have. Finally 9 % of hydrometeors fulfill the criterion that the height measured in camera A is not more than 20 % different to the height measured in camera B (Table 3).

Figure 13 a to c summarizes the performance evaluation in case of real solid phase precipitation. The measured mean shape parameters show the following correlations: Higher elongation means lower roundness and shape factor. Lower elongation means higher roundness and shape factor. Intervals with lower roundness also have lower shape factors and vice versa.

## 4 Discussion

### 4.1 Calibration

The reason for the systematic deviation registered in the calibration experiment can be a small miss alignment of the optical elements caused by transportation or small deformations of the housing through strong winds. Because of the constant overestimation of the measured quantity expressed in the intercept t of the regression line a correction procedure is implemented for the pixel width. After the correction the nominal and measured values agree very well (Fig. 8). The mentioned deviation in the size measurement leads to the recommendation to all 2DVD users to recalibrate their instrument periodically.

### 4.2 Measurement ranges and uncertainties

With a certain threshold partially shaded pixels in the 2DVD images are counted as fully shaded or fully non shaded. This introduces a non avoidable error to every size related 2DVD measurement that grows with decreasing size of the detected object





AMTD
8, 3087–3120, 2015

(Fig. 9). For reliable shape and size measurements with a 2DVD it is recommended to take only particles with a maximum dimension of at least 0.5 mm for data evaluation. Size and shape characterization with a relative standard deviation of less than 5 % is only possible for particles larger than 1 mm. For particles between 0.5 and 1.0 mm the relative standard deviation can grow up to 22 % for the volume, 17 % for size parameters and 14 % for shape descriptors.

### 4.3 Validation of 2DVD measurements

The measurement results with the solid spheres reveal how well shape, size and velocity information gained with 2DVD measurements reproduce the reality.

a. The expected value of the **elongation** $E = 1$ is reproduced very well by the 2DVD measurements (Fig. 10a and b). The outliers at 0.5, 2, 3, 4 and 5 mm are single measurements where partially shadowed edge pixels artificially increase the width.

b. Especially for the larger spheres the expected **roundness** value of $R = 1$ is reproduced very well. With smaller diameters the influence of the pixel shaped edge gets larger. As a consequence the measured shape deviates more from a sphere and the values are spread more widely (Fig. 10c and d).

c. The expected value for the **shape factor** of a sphere is $S = 1$. The measured values are between 0.6 and 0.7. The reason for this deviation is the pixel shaped perimeter of the pictures. The perimeter of a konvex pixel shaped object is always equal to the perimeter of the surrounding rectangle. For example a spherical object with a pixel shaped edge and a diameter of 6 mm has a theoretically calculated shape factor of 0.62. Using a blurring edge filter that spreads over 20 pixels before detecting the perimeter of the object improves the the shape factors to values between 0.90 and 0.95 (Fig. 10 e to h). Especially for solid precipitation





AMTD
8, 3087–3120, 2015

particles with very fine features image processing with a blurring edge filter is not recommended. The risk of loosing important information is too high.

d. The measurement quality of the **maximum dimension** (Fig. 8),

e. **equivalent diameters** (Fig. 11a) and

f. **volumes** is excellent for particles larger than 0.5 mm (Fig. 11b).

g. The comparison between measured and theoretically calculated vertical **fall velocity** shows very good agreement (Fig. 11c).

In the experiment with styrofoam particles the mismatch probability was below 2.5 %. For particles with sizes below 3 mm the theoretical prediction for spherical particles with a density of 270.0 kg $m^{-3}$ is plotted in Fig. 12. The particles with sizes around 2 mm follow this prediction very well. The measured size and velocity depends strongly on the orientation of the particle. For this reason a small spread around the single measurements has to be accepted.

For results without matching artifacts it is essential to introduce a suitable matching algorithm. The original matching algorithm produces a large amount of mismatches. Less than 9 % of the registered events fulfill the criteria to be simultaneously detected hydrometeors by both cameras (Table 3). For shape parameter measurements in case of real solid phase precipitation, the 2DVD shows the expected correlations (Fig. 13a to c).

## 5 Conclusions

The results show that state of the art 2-D-video disdrometer technique is suitable for detailed characterization of hydrometeor size, velocity and shape parameters. Taking the shape factor for shape characterization of hydrometeors it is important to consider the large influence of the pixel shaped perimeter. The user of this technique should





AMTD
8, 3087–3120, 2015

keep in mind that size and shape characterization with a relative standard deviation of less than 5 % is only possible for particles larger than 1 mm. For mixed and solid phase hydrometeors it is essential to implement a suitable matching algorithm to avoid errors in shape and velocity measurements through matching artifacts.

*Acknowledgements.* We thank the staff of UFS Schneefernerhaus for assistance in the operation of the 2DVD.

The study was supported by the German Ministry of Science and Education (BMBF) under contract 02NUK15B. Its contents are solely the responsibility of the authors.

## References

Atlas, D., Shrivastava, R., and Sekhon, R.: Doppler radar characteristics of precipitation at vertical incidence, Rev. Geophys. Space Ge., 11, 1–35, 1973. 3091, 3092

Barthazy, E. and Schefold, R.: Fall velocity of snowflakes of different riming degree and crystal types, Atmos. Res., 82, 391–398, 2006. 3089, 3091

Barthazy, E., Goke, S., Schefold, R., and Högl, D.: An optical array instrument for shape and fall velocity measurements of hydrometeors, J. Atmos. Ocean. Tech., 21, 1400–1416, 2004. 3089

Battaglia, A., Rustmeier, E., Tokay, A., Blahak, U., and Simmer, C.: PARSIVEL snow observations: a critical assessment, J. Atmos. Ocean. Tech., 27, 333–344, 2010. 3089

Brandes, E. A., Ikeda, K., Zhang, G., Schönhuber, M., and Rasmussen, R. M.: A statistical and physical description of hydrometeor distributions in Colorado snowstorms using a video disdrometer, J. Appl. Meteorol. Clim., 46, 634–650, 2007. 3089

Feind, R. E.: Comparison of Three Classification Methodologies for 2D Probe Hydrometeor Images Obtained from the Armored T-28 Aircraft, Tech. Rep. SDSMT/IAS/R08-01, Institute of Atmospheric Sciences, South Dakota School of Mines and Technology, Rapid City, SD, USA, 2008. 3089

Frank, G., Härtl, T., and Tschiersch, J.: The pluviospectrometer: classification of falling hydrometeors via digital image processing, Atmos. Res., 34, 367–378, 1994. 3089





AMTD

8, 3087–3120, 2015

On the potential of 2-D-Video Disdrometer technique

F. Bernauer et al.

Grazioli, J., Tuia, D., Monhart, S., Schneebeli, M., Raupach, T., and Berne, A.: Hydrometeor classification from two-dimensional video disdrometer data, Atmos. Meas. Tech., 7, 2869–2882, doi:10.5194/amt-7-2869-2014, 2014. 3089, 3093
Gunn, R. and Kinzer, G. D.: The terminal velocity of fall for water droplets in stagnant air, J. Meteorol., 6, 243–248, 1949. 3091
Hanesch, M.: Fall Velocity and Shape of Snowflakes, PhD thesis, Supervisor: A. Waldvogel, Swiss Federal Institute of Technology, Zürich, 1999. 3091, 3092, 3096, 3105
Hiroshi, I.: Radar backscattering computations for fractalshaped snowflakes, J. Meteorol. Soc. Jpn., 86, 459–469, 2008. 3089
Huang, G. J., Bringi, V. N., Cifelli, R., Hudak, D., and Petersen, W. A.: A methodology to derive radar reflectivity–liquid equivalent snow rate relations using C-band radar and a 2D Video Disdrometer, J. Atmos. Ocean. Tech., 27, 637–651, 2010. 3089, 3091, 3092
Jiao, L. and Liu, Y.: Analyzing the shape characteristics of land use classes in remote sensing imagery, ISPRS Annals of Photogrammetry, Remote Sens. Spatial Inf. Sci., I-7, 135–140, 2012. 3093
Kruger, A. and Krajewski, W. F.: Two-dimensional video disdrometer: a description, J. Atmos. Ocean. Tech., 19, 602–617, 2002. 3089, 3091
Kyrö, E.-M., Grönholm, T., Vuollekoski, H., Virkkula, A., Kulmala, M., and Laakso, L.: Snow scavenging of ultrafine particles: field measurements and parameterization, Boreal Environ. Res., 6095, 527–538, 2009. 3089
Locatelli, J. D. and Hobbs, P. V.: Fall speeds and masses of solid precipitation particles, J. Geophys. Res., 79, 2185–2197, 1974. 3091
Löffler-Mang, M. and Joss, J.: An optical disdrometer for measuring size and velocity of hydrometeors, J. Atmos. Ocean. Tech., 17, 130–139, 2000. 3089
Paramonov, M., Grönholm, T., and Virkkula, A.: Below-cloud scavenging of aerosol particles by snow at an urban site in Finland, Boreal Environ. Res., 16, 304–320, 2011. 3089
Schaefer, V. J.: The preparation of snow crystal replicas-VI, Weatherwise, 9, 132–135, 1956. 3089
Schuur, T. J., Ryzhkov, A. V., Zrnic, D. S., and Schonhuber, M.: Drop size distributions measured by a 2D video disdrometer: comparison with dual-polarization radar data, J. Appl. Meteorol., 40, 1019–1034, 2001. 3089
Sportisse, B.: A review of parameterizations for modelling dry deposition and scavenging of radionuclides, Atmos. Environ., 41, 2683–2698, 2007. 3089





AMTD
8, 3087–3120, 2015

On the potential of 2-D-Video Disdrometer technique

F. Bernauer et al.

Thurai, M. and Bringi, V. N.: Drop axis ratios from a 2D video disdrometer, J. Atmos. Ocean. Tech., 22, 966–978, 2005. 3089
Thurai, M., Szakall, M., Bringi, V. N., Beard, K. V., Mitra, S., and Borrmann, S.: Drop shapes and axis ratio distributions: comparison between 2D video disdrometer and wind-tunnel measurements, J. Atmos. Ocean. Tech., 26, 1427–1432, 2009. 3089
Thurai, M., Williams, C. R., and Bringi, V. N.: Examining the correlations between drop size distribution parameters using data from two side-by-side 2D-video disdrometers, Atmos. Res., 144, 95–110, 2014. 3089
Tokay, A., Kruger, A., and Krajewski, W. F.: Comparison of drop size distribution measurements by impact and optical disdrometers, J. Appl. Meteorol., 40, 2083–2097, 2001. 3089
Xue, M., Droegemeier, K. K., and Wong, V.: The Advanced Regional Prediction System (ARPS); a multi-scale nonhydrostatic atmospheric simulation and prediction model. Part I: Model dynamics and verification, Meteorol. Atmos. Phys., 75, 161–193, 2000. 3088
Zhang, G., Xue, M., Cao, Q., and Dawson, D.: Diagnosing the intercept parameter for exponential raindrop size distribution based on video disdrometer observations: model development, J. Appl. Meteorol. Clim., 47, 2983–2992, 2008. 3089
Zhang, G., Luchs, S., Ryzhkov, A., and Xue, M.: Winter precipitation microphysics characterized by polarimetric radar and video disdrometer observations in central Oklahoma, J. Appl. Meteorol. Clim., 50, 1558–1570, 2011. 3089
Zikmunda, J.: Fall velocities of spatial crystals and aggregates, J. Atmos. Sci., 29, 1511–1515, 1972. 3089





AMTD
8, 3087–3120, 2015

On the potential of 2-D-Video Disdrometer technique

F. Bernauer et al.

**Table 1.** The filter criteria for the test of the original matching algorithm are adapted from Hanesch (1999).

| Filter type |
|---|
| $D > 0.2$ mm (spatial resolution, sr) |
| sr + Velocity: $0.5\,\text{m}\,\text{s}^{-1} < v < 6.0\,\text{m}\,\text{s}^{-1}$ |
| sr + Velocity: $v(D) < v_{\text{Rain}}(D)$ |
| sr + Geometry: $0.1 < H/W < 10.0$ |
| $0.1 < W_A/W_B < 10.0$ |
| sr + $H_A - H_B < 0.2\,H_{max}$ |



AMTD

8, 3087–3120, 2015

On the potential of 2-D-Video Disdrometer technique

F. Bernauer et al.

**Table 2.** Results of the calibration measurements with steel spheres. *m* and *t* denote the slope and intercept of the regression line, respectively. *r* is the correlation coefficient.

| | $m$ | $t$ | $r^2$ |
|---|---|---|---|
| $H_A$ | 1.04 | 0.35 | 0.998 |
| $H_B$ | 1.03 | 0.38 | 0.998 |
| $W_A$ | 1.04 | 0.35 | 0.998 |
| $W_B$ | 1.03 | 0.37 | 0.998 |





AMTD
8, 3087–3120, 2015

**Table 3.** Contribution of detected hydrometeors after applying the original matching algorithm.

| Filter type | Remaining number of flakes | % |
|---|---|---|
| Total (no filter) | 439 072 | 100 |
| $D > 0.2$ mm (spatial resolution, sr) | 178 949 | 40.8 |
| sr + Velocity: $0.5\,\mathrm{m\,s^{-1}} < v < 6.0\,\mathrm{m\,s^{-1}}$ | 142 299 | 32.4 |
| sr + Velocity: $v(D) < v_{\mathrm{Rain}}(D)$ | 111 896 | 25.5 |
| sr + Geometry: $0.1 < H/W < 10.0$ $0.1 < W_A/W_B < 10.0$ | 86 185 | 19.6 |
| sr + $H_A - H_B < 0.2\,H_{max}$ | 38 677 | 8.8 |



Discussion Paper | Discussion Paper | Discussion Paper | Discussion Paper |

AMTD

8, 3087–3120, 2015

On the potential of 2-D-Video Disdrometer technique

F. Bernauer et al.

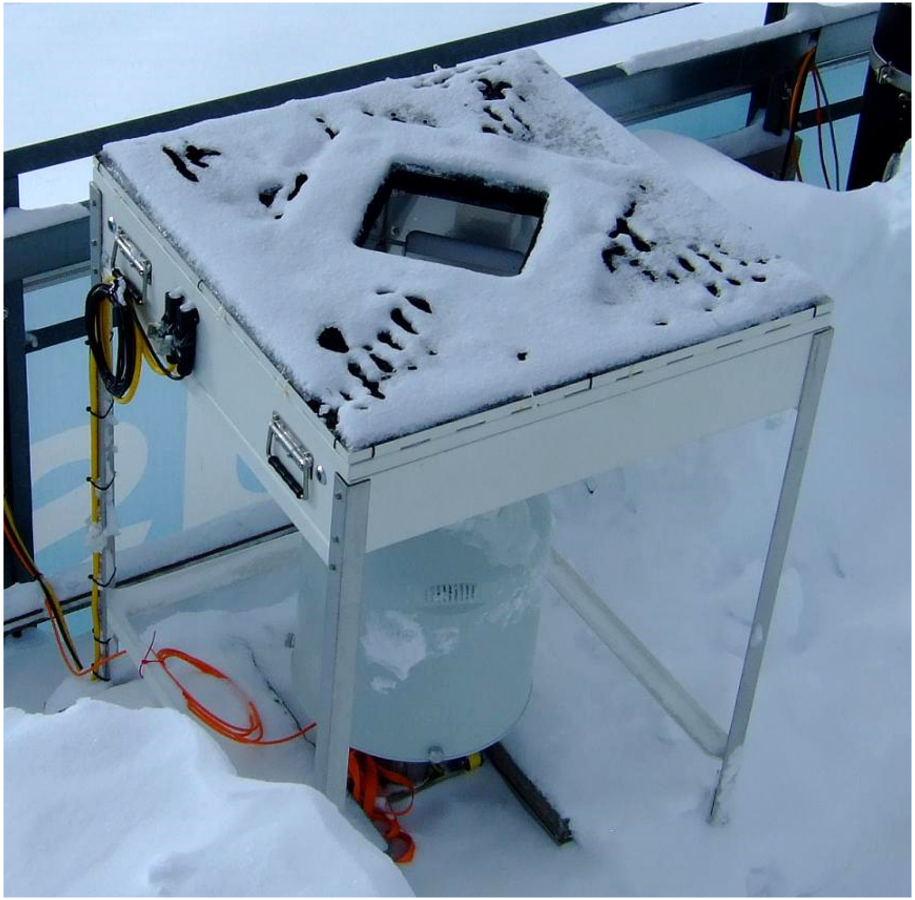

**Figure 1.** The Compact 2DVD top has a flat housing design which makes it less sensitive to horizontal winds. Below the sensitive area a weighing precipitation gauge is mounted.





AMTD
8, 3087–3120, 2015

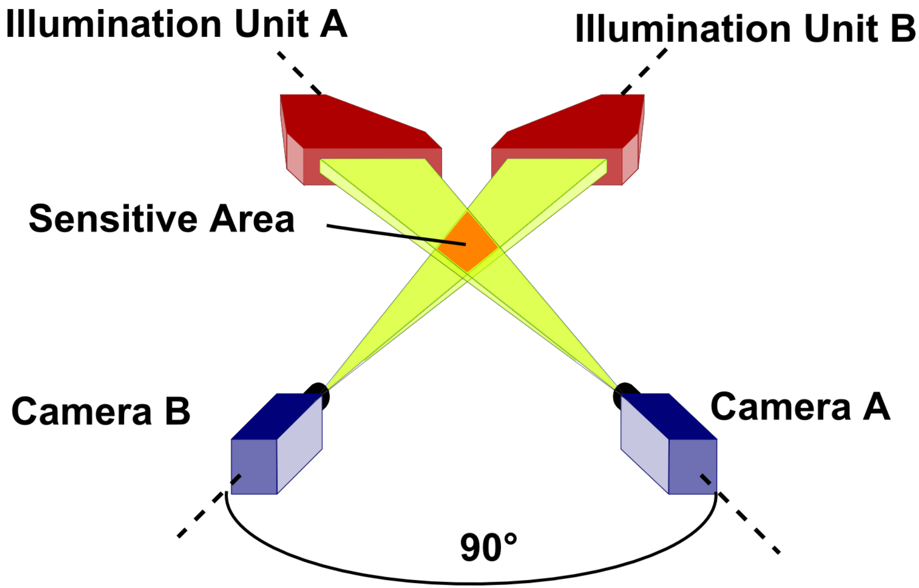


**Figure 2.** Measurement prinziple of the 2DVD.





AMTD
8, 3087–3120, 2015

On the potential of 2-D-Video Disdrometer technique

F. Bernauer et al.

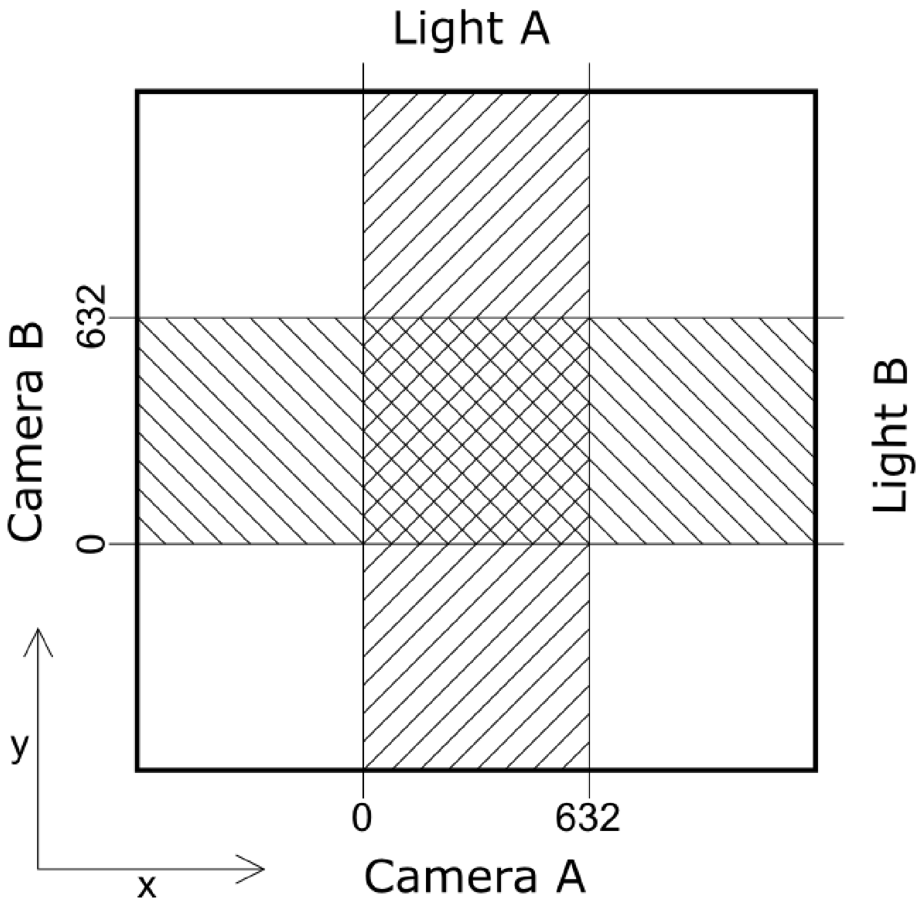


**Figure 3.** A schematic view of the 2DVD measuring area seen from above.





AMTD
8, 3087–3120, 2015

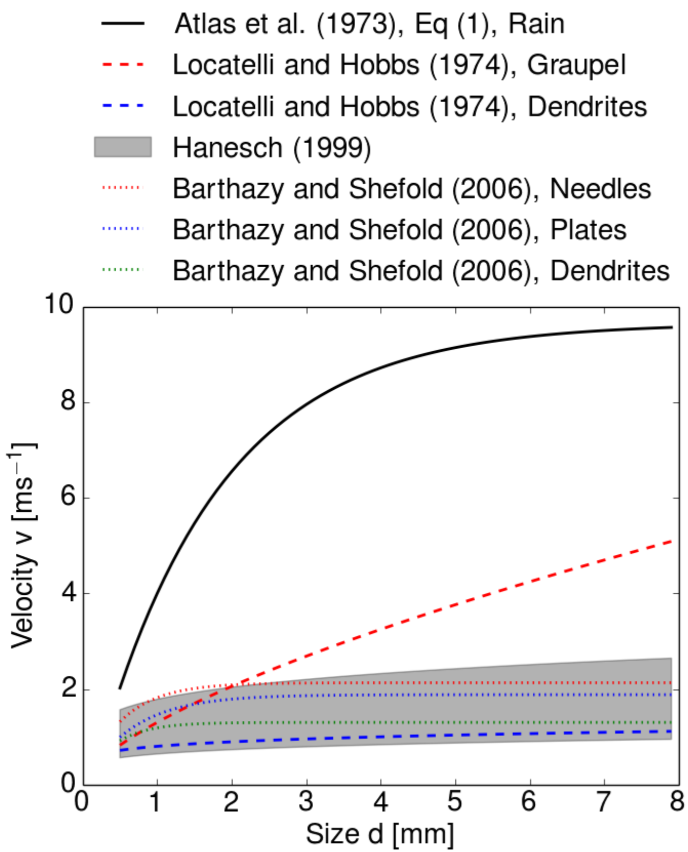


**Figure 4.** Size–velocity relationships for different types of hydrometeors as reported in literature. The term *size* means *diameter* in case of rain, in case of snow it means *height* or *maximum dimension*.





AMTD
8, 3087–3120, 2015

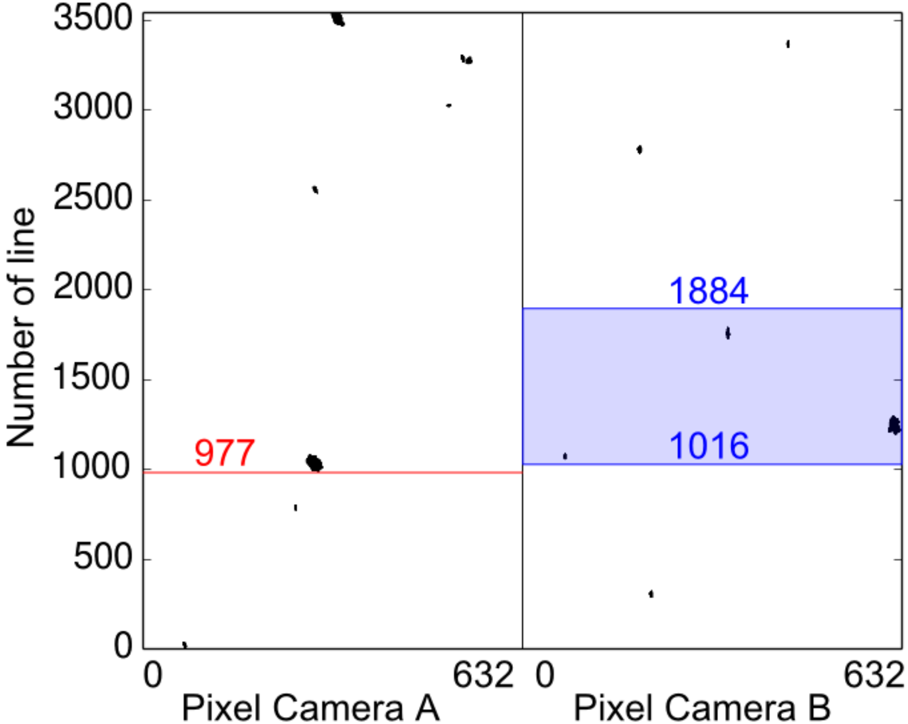


**Figure 5.** This example shows two raw camera streams. For the specific snowflake hitting camera A at the red line, all possible matching partners in camera B are within the shaded region.





AMTD
8, 3087–3120, 2015



F. Bernauer et al.

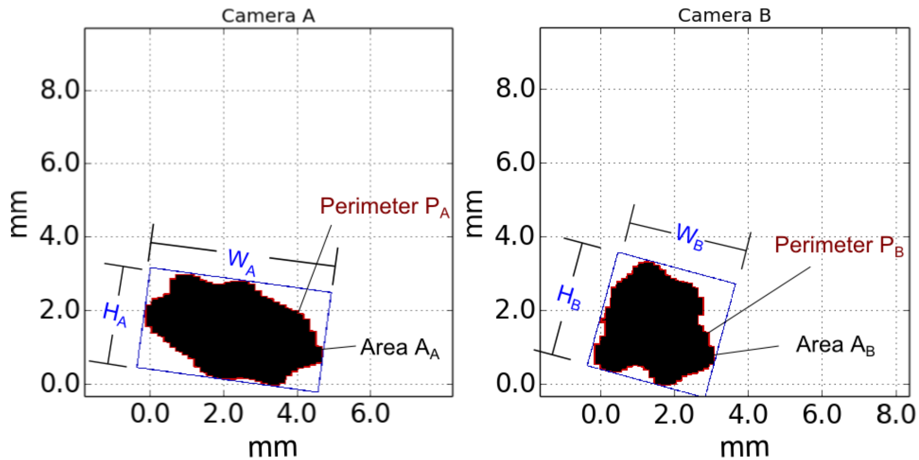


**Figure 6.** The definition of width ($W$), height ($H$), perimeter ($P$) and area ($A$) for a hydrometeor as recorded with the 2DVD.





AMTD
8, 3087–3120, 2015

On the potential of 2-D-Video Disdrometer technique

F. Bernauer et al.


**Figure 7.** Fourteen styrofoam particles with maximum dimensions from 2 to 15 mm simulate solid hydrometeors to validate the matching algorithm.





AMTD
8, 3087–3120, 2015

On the potential of 2-D-Video Disdrometer technique

F. Bernauer et al.

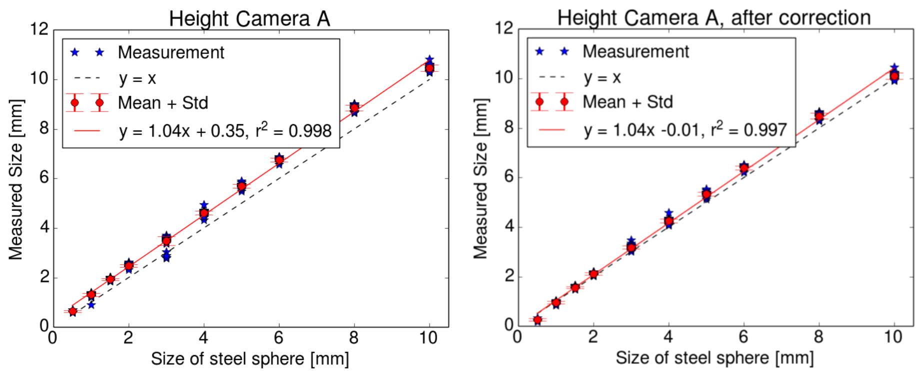


**Figure 8.** Comparison between nominal and measured height of calibration spheres before and after correcting the pixel width.





AMTD
8, 3087–3120, 2015

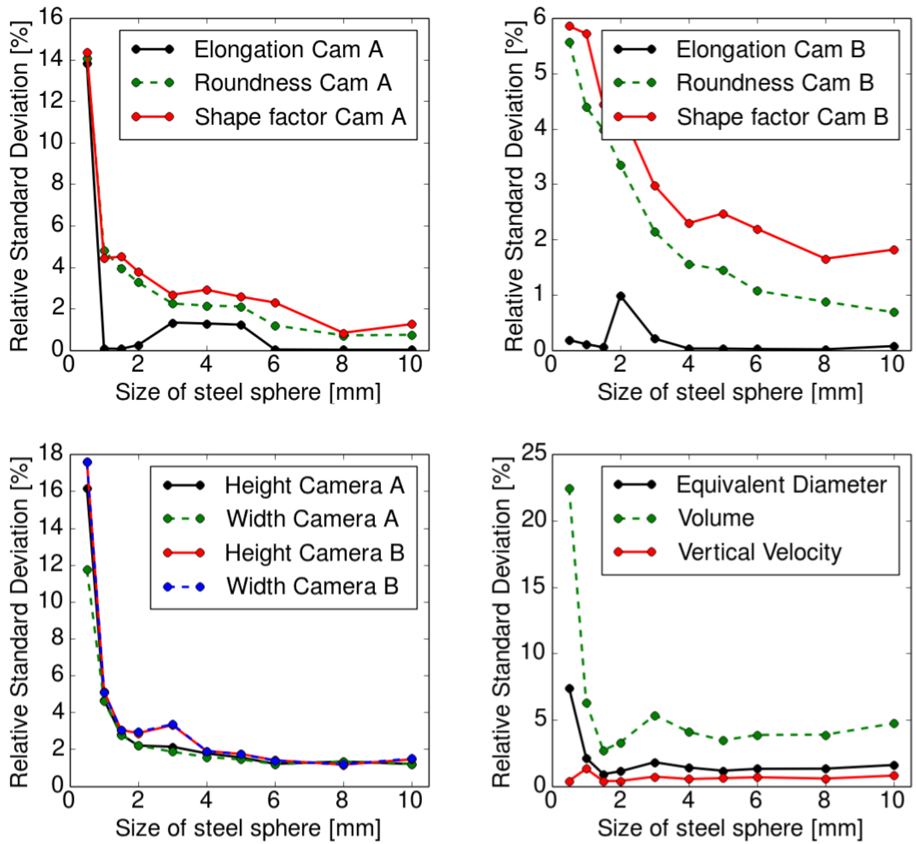


**Figure 9.** The relative standard deviation for the different quantities measured with steel spheres. As a direct consequence of vertical and horizontal quantization the relative standard deviation rises with smaller diameters.





AMTD
8, 3087–3120, 2015

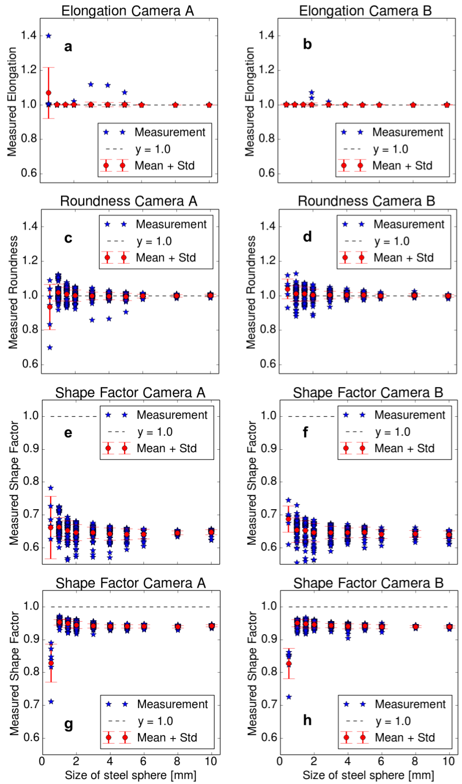


**Figure 10.** The expected values for $E = R = 1$ for the calibration spheres are reproduced very well (**a** to **d**). The measured shape factor for the calibration spheres lays between 0.6 and 0.7 (**e** and **f**). The expected value is 1. After treatment with a blurring edge filter it lays between 0.90 and 0.95 (**g** and **h**).





AMTD
8, 3087–3120, 2015



F. Bernauer et al.

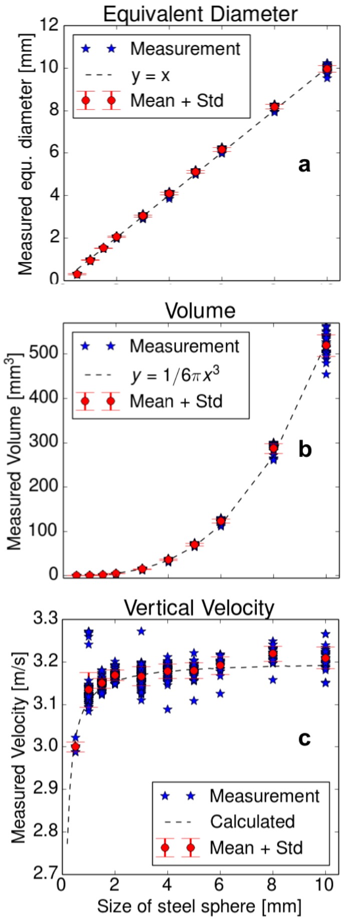


**Figure 11.** Volumes and equivalent diameters of the solid spheres are reproduced very well in 2DVD measurements (**a** and **b**). The comparison between measured and theoretically calculated vertical fall velocity shows good agreement **(c)**.





AMTD
8, 3087–3120, 2015

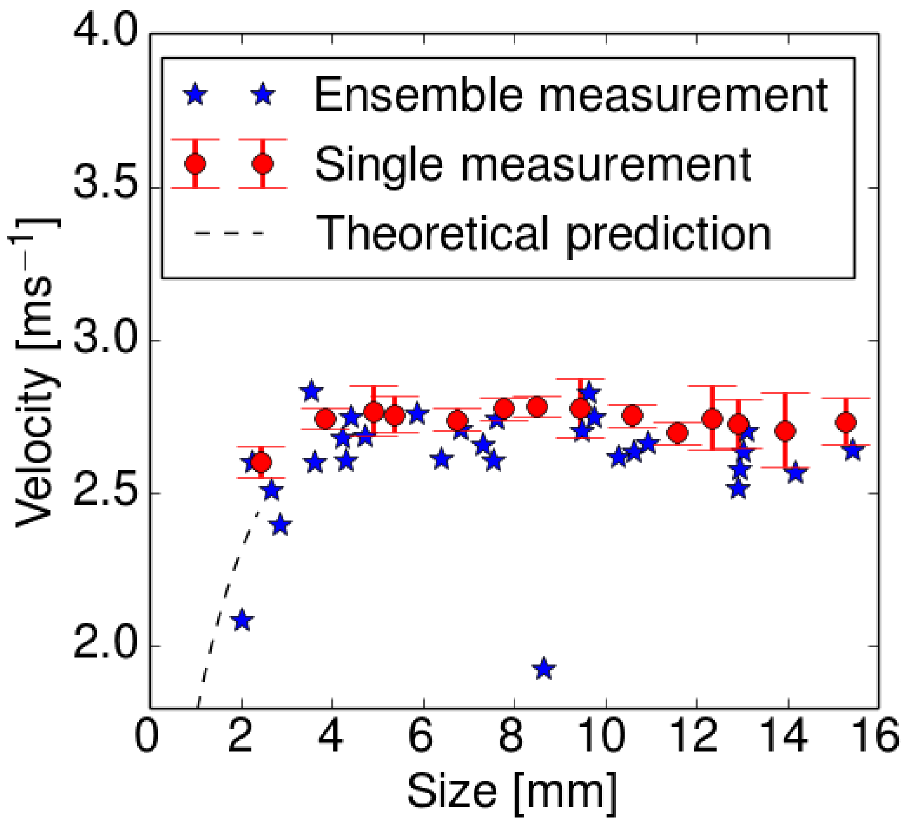


**Figure 12.** Good performance of the matching algorithm is shown by comparing velocity measurements of single styrofoam objects (dropped one after the other) and of the whole ensemble (all particles dropped at the same time from the same height).





AMTD
8, 3087–3120, 2015

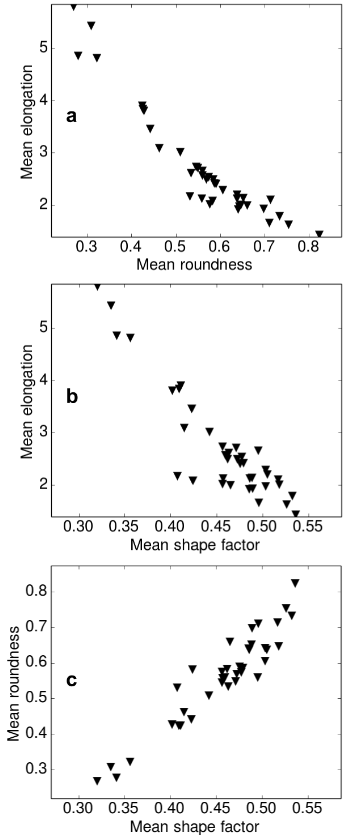


**Figure 13.** Comparing mean shape parameters measured for real snowflakes shows very self-consistent behavior. Higher elongation means lower roundness **(a)** and lower shape factor **(b)**, lower roundness means lower shape factor **(c)** (and vice versa).





AMTD
8, 3087–3120, 2015

On the potential of 2-D-Video Disdrometer technique

F. Bernauer et al.

Title Page
Abstract | Introduction
Conclusions | References
Tables | Figures
Back | Close
Full Screen / Esc
Printer-friendly Version
Interactive Discussion